JOURNAL OF APPLIED ELECTROCHEMISTRY 1 (1971) 231–243

REVIEW

Fundamental and applied aspects of the electrochemistry of chlorine

G. BIANCHI

Laboratory of Electrochemistry and Metallurgy, University of Milan, Milan, Italy

Received 19 April 1971; revised MS received 8 July 1971

Data so far published on the thermodynamics of sodium amalgams and chloride solutions allow us to calculate the reversible potential for the electrolysis of brines at concentrations and temperatures corresponding to industrial processing. Data are also reported for the electrolysis of hydrochloric acid solutions. Kinetics of chlorine discharge and passivation phenomena on Pt, Pt–Ir and oxide-based electrodes are reviewed, in relation to the use of dimensionally stable electrodes, on titanium supports. The electronic conduction of RuO_2 and other oxides is also discussed.

Introduction

The production of chlorine is continually expanding, the average annual growth rate being 8% for the U.S.A. during the 1959–1969 decade. Again in the U.S.A., chlorine production increased by 11·2% from 1968 to 1969, the record value being 9,427,000 tons [1]. The Italian production of chlorine for 1969 was 782,806 tons with an increase of 4% with respect to 1968 [2]. About 60% of the chlorine produced is utilized by the plastics industry, chiefly for P.V.C. production [3] which leads to hydrochloric acid as a by-product. The *chemical* conversion of hydrochloric acid into chlorine (Deacon process and derivatives) or into organic chloroderivatives (oxychloridation process) has not, so far, reached such proportions as to be significantly competitive with the electrolytic production of chlorine.

With regard to the electrolytic production of chlorine from hydrochloric acid solutions, a process which is still in the course of development, its interesting aspects are chiefly linked with pollution problems. In fact, electrolysis is the simplest way, well utilizable on a small-scale, for disposing the by-product hydrochloric acid and avoiding expensive treatments for the neutralization of dumps.

The electrolysis of sodium chloride solutions in diaphragm cells has undergone important modifications during the last decade, implying increases of both current densities and cell currents, but leaving nearly unchanged the specific consumptions per kg of chlorine. Table 1

Table 1. Some typical data on the evolution of diaphragm cells.

Year	1940	1950	1970
Power d.c., kWh/ton Cl_2	3,370	3,640	3,450
Current/cell, kA	25	25	70
Anodic current density A/m²	900	1,200	1,300
Voltage across cell, V	4·4	4·75	4·5

in particular indicates the decrease in specific consumptions recently obtained, in spite of the increase of current densities, by means of the introduction of non-consumable electrodes (DSA).

As can be seen in Table 2, the evolution of the mercury cells was even more significant. The introduction of silicon rectifiers permitted a large increase in cell currents together with a drastic reduction of mercury hold-up; further,

Table 2 Some typical data on the evolution of mercury cells

Year	1950	1970
Power d.c., kWh/ton Cl_2	3,600	3,400
Anodic current density, A/m^2	3,700	13,000
Mercury consumption gg. Hg/ton Cl_2	1,000	50
Mercury hold-up kg/kA cell	57	12
Current/cell kA	30	500

the introduction of non-consumable titanium electrodes permitted a reduction in the specific consumption in spite of the large increase of current densities.

From the data in Tables 1 and 2 it is evident that, due to the present high demand for chlorine from the chemical industries, the recent technological evolution has been oriented towards an increased production capacity by the plants and to the reduction of the specific power consumption, a reduction which could, however, have been made possible by new technologies. During the last decade, in the Laboratory of Electrochemistry and Metallurgy of the University of Milan, a research programme has been developed with the aim of obtaining basic thermodynamic and kinetic data as necessary supports for the improvement of the technology of the electrolytic production of chlorine.

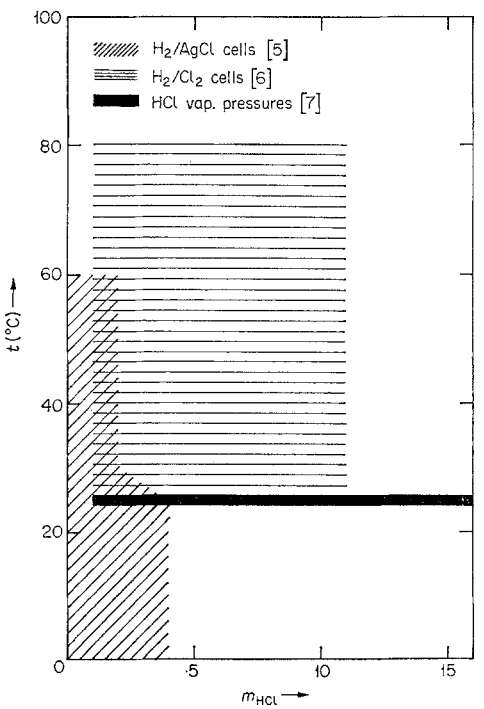

Fig. 1. Activity coefficients of aqueous HCl. Ranges of temperature and molality covered by Harned and Ehlers [5], Mussini *et al.* [6], and Randall and Young [7].

As concerns Electrochemical Thermodynamics, a survey of the data now available leads to the following synopsis.

The standard potential of the chlorine electrode, which was known only at room temperature, was recently determined over a range up to 80°C [4]. Fig. 1 shows the present overall situation for the determination of activity coefficients of hydrochloric acid at high concentrations and temperatures. For the activity coefficients of sodium chloride solutions, data at low temperature (obtained from emf methods) and data at high temperature (boiling point method) were available. Recently, as shown in Fig. 2, it has

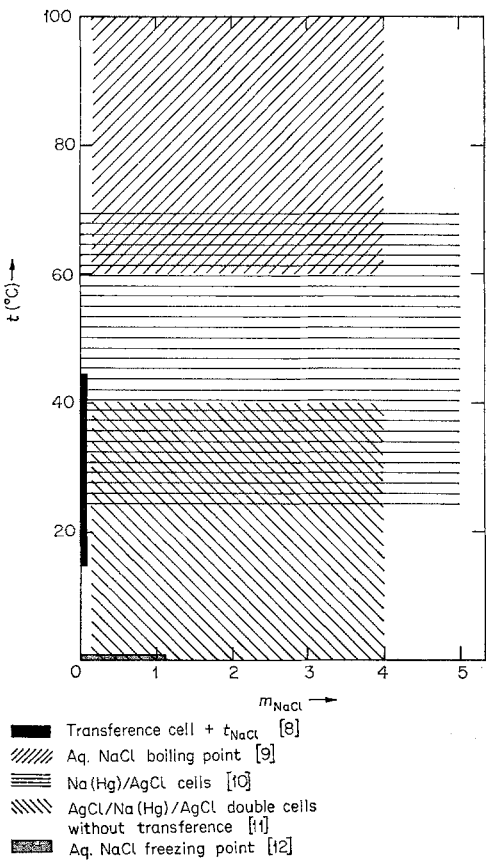

Fig. 2. Activity coefficients of aqueous NaCl. Ranges of temperature and molality covered by Janz and Gordon [8], Smith and Hirtle [9], Mussini and Pagella [10], Harned and Nims [11], and Scatchard and Prentiss [12].

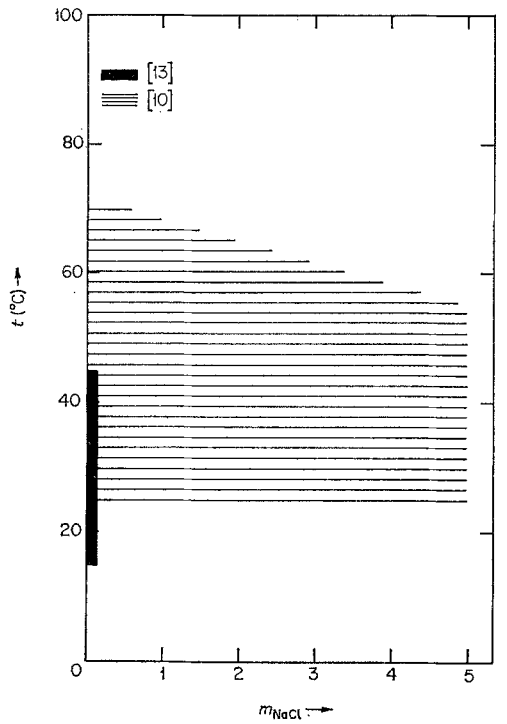

Fig. 3. Transference numbers of aqueous NaCl. Ranges of temperature and concentration covered by Allgood and Gordon [13], and by Mussini and Pagella [10].

been possible, by the emf method, to obtain the data for high NaCl concentration up to 70°C. The transference numbers of sodium chloride solutions are, at present, known over the concentration and temperature ranges visualized in Fig. 3. The data on the sodium activities in sodium amalgams are now also known at higher concentrations and temperatures, as shown in Fig. 4.

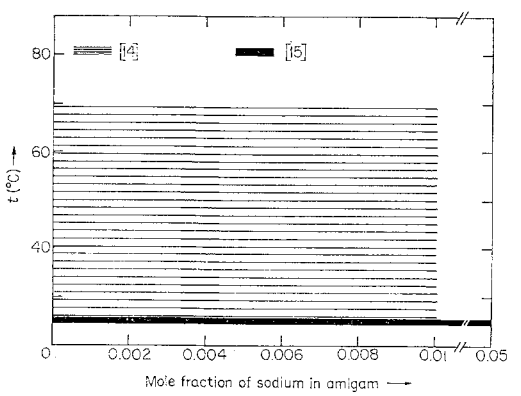

Fig. 4. Activity coefficients of sodium in amalgam. Ranges of temperature and amalgam composition covered by Mussini *et al.* [14], and by Dietrick, Yeager and Hovorka [15].

Thus a reconsideration of the fundamental and applied aspects of the electrochemistry of chlorine must be based on the data concerning the operating conditions for the industrial production of chlorine which have been obtained only recently.

Thermodynamics of processes of electrolysis in HCl solutions

The solution of this problem was made possible by the setting up of hydrogen and chlorine electrodes capable of working satisfactorily in concentrated and hot solutions of HCl, i.e. under conditions where the solubilities of AgCl and Hg_2Cl_2 in HCl make it impossible to use silver-chloride or calomel electrodes. By use of the hydrogen electrode [16], a development of porous electrodes for fuel cells [17], a very extended surface for the triple contact solution–catalyst–gas may be obtained. It consists of a horizontal porous-graphite disc on the upper surface of which stands a layer of platinum black kneaded with a small amount of PTFE (Fig. 5). The high reversibility of this hydrogen

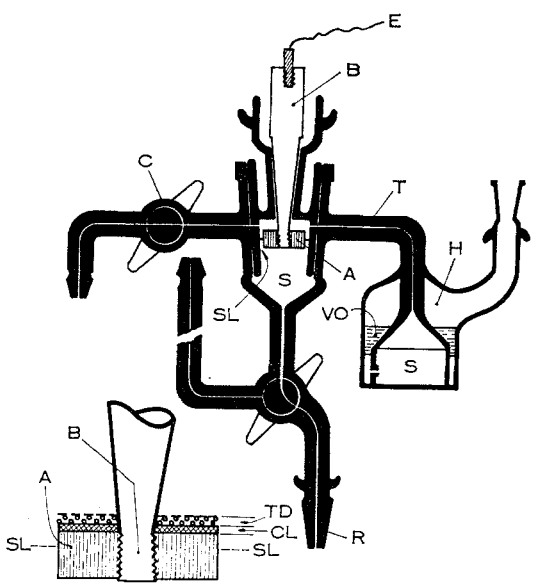

Fig. 5. Structure of the hydrogen electrode: A, porous graphite disc; B, screw stem of impermeabilized graphite; C, gas inlet stopcock; CL, catalyst layer; E, electrical connection; H, hydraulic seal; R, to second half-cell; S, solution; SL, solution level; T, tube connecting to hydraulic seal; TD, Teflon drop network; VO, vacuum oil layer on solution. (From G. Bianchi *et al J. Electrochem. Soc.*, **112** (1965) 921.)

electrode is demonstrated by an exchange current as high as 30·0 mA/cm^2 in 6·06 M HCl at 25°C. Stability and reproducibility turn out to be better than 30 μV when the electrode is freshly prepared, and better than 10μV after ageing.

The chlorine electrode [4] has been developed by making use of the corrosion resistance of platinum–iridium alloys, with 45% iridium, in concentrated and hot chlorine-saturated HCl solutions. The impossibility of obtaining such alloy in the form of wires or sheets has been overcome by preparing it by thermal decomposition of platinum and iridium salts on a tantalum sheet. The electrode has been constructed according to the scheme in Fig. 6, leading to an exchange current of 16 mA/cm^2 in 1·75 HCl at 25°C. Stability and reproducibility of these chlorine electrodes was better than 10 μV.

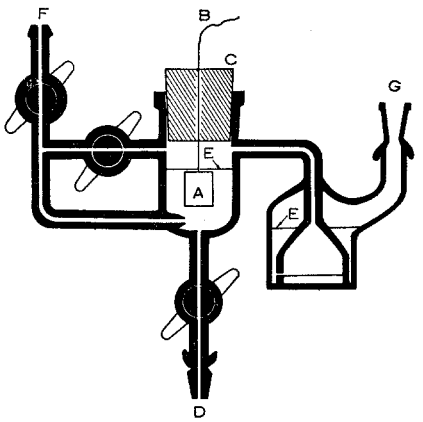

Fig. 6. Structure of the chlorine half-cell: A, electrode substrate consisting of a tantalum foil coated with a Pt–Ir alloy; B, electrical connection to potentiometer; C, polytetrafluoroethylene plug; D, connection to the silver/silver-chloride half cell; E, solution level; F, chlorine inlet; G; chlorine outlet. (From G. Faita *et al J. Electrochem. Soc.*, **114** (1967) 340.)

The cell $H_2/HCl/Cl_2$ was used for two complementary purposes, in one case [18] keeping a constant HCl concentration in solution and varying the partial pressure of chlorine, in the other case [6] keeping a constant chlorine pressure but varying the HCl concentration.

For a HCl solution in the presence of chlorine the following equilibria exist

$$Cl_2\ (gas) + Cl^-\ (aq) \rightleftharpoons Cl_3^-\ (aq) \qquad (1)$$

$$Cl_2\ (aq) + Cl^-\ (aq) \rightleftharpoons Cl_3^-\ (aq) \qquad (2)$$

with corresponding equilibrium constants K_1 and K_2. If p_{Cl_2} is the partial pressure of chlorine, m is the molal concentration of HCl in solution and γ is the corresponding mean molal activity coefficient (obtained at different temperatures as explained below) the emf of the above cell is given by

$$E = E_G^\circ + \frac{RT}{2F}\ln(p_{Cl_2}) - \frac{2RT}{F}\ln(m\gamma_\pm)_{HCl} + \frac{RT}{F}\ln(1 + K_1 p_{Cl_2})$$

in terms of equilibrium (1), E_G° being the standard potential referred to the Cl_2 (gas)/Cl^- couple. Rearranging, after linearizing the last logarithmic term,

Table 3. Standard potentials of the chlorine electrode, referred to the Cl_2 (gas)/Cl^- (E_G°) and to the Cl_2(aq)/Cl^- (E_A°) couples, and equilibrium constants of reactions (1) *and* (2), *at various temperatures.**

t(°C)	$E_G^\circ(V)$	$E_A^\circ(V)$	K_1	K_2
25	1·35827 ± 0·00002 (a)	1·396 ± 0·002 (a)	0·0119 ± 0·0009 (a)	0·215 ± 0·022 (a)
	1·35852 (b)	1·39 (c)	0·010 (d)	0·176 (d)
				0·191 (e)
40	1·33910 ± 0·00002 (a)	1·384 ± 0·004 (a)	0·0064 ± 0·0009 (a)	0·18 ± 0·03 (a)
	1·33919 (b)	—	—	—
60	1·31154 ± 0·00001 (a)	1·366 ± 0·006 (a)	0·0032 ± 0·0007 (a)	0·14 ± 0·03 (a)
	1·31144 (b)	—	—	—
80	1·28172 ± 0·00001 (a)	1·344 ± 0·036 (a)	0·0012 ± 0·0010 (a)	0·07 ± 0·06 (a)
	1·28153 (b)	—	—	—

* Sources of data as indicated. (a) from ref. [18]; (b) from ref. [6]; (c) from ref. [19]; (d) from ref. [20]; (e) from ref. [21].

$$\frac{EF}{RT} + 2\ln(m\gamma_{\pm})_{HCl} - \tfrac{1}{2}\ln(p_{Cl_2}) = \Psi$$

$$= \frac{FE^{\circ}_G}{RT} + K_1 p_{Cl_2}$$

is obtained.

Then by plotting Ψ against p_{Cl_2} one should (and actually does) obtain straight lines corresponding to the different temperatures of experiments. The slopes of these straight lines give K_1, while from the intercepts at $p_{Cl_2} = 0$ one gets E°_G (cf. Fig. 7). From parallel determinations of chlorine solubility at various p_{Cl_2} and temperatures, it is also possible to deduce the K_2 values.

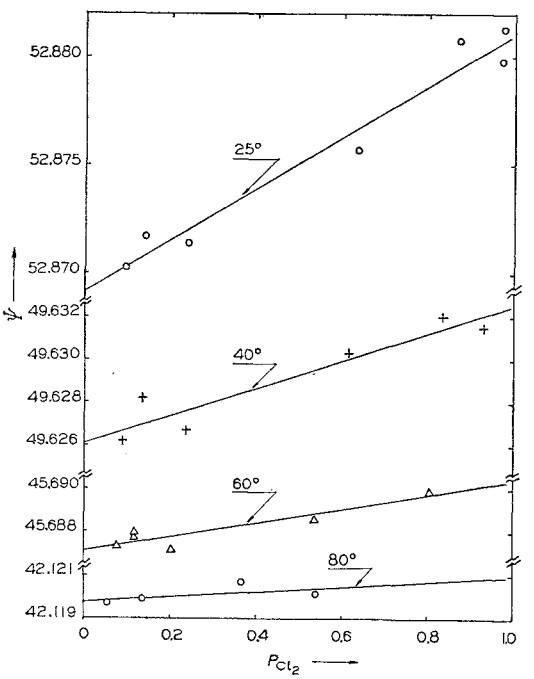

Fig. 7. Simultaneous determination of E_G for the couple Cl_2 (gas)/Cl^- and of K_2 for the process $Cl_2(g) + Cl^- = Cl_3^-$ by extrapolating the function Ψ to $P_{Cl_2} = 0$. (From A. Cerquetti *et al.*, *J. Electroanal. Chem.*, **20**, (1969) 411.)

H_2, 1 atm | HCl, $1M$ | Cl_2, p atm

$Cl_2(gas) + Cl^-(aq) \rightleftharpoons Cl^-(aq)$ $\quad K_1 = m_{Cl_3^-}\gamma_{Cl_3^-}/(p_{Cl_2} m_{Cl^-} {}^{*}\gamma_{Cl^-})$

$Cl_2(aq) + Cl^-(aq) \rightleftharpoons Cl_3^-(aq)$ $\quad K_2 = m_{Cl_3^-}\gamma_{Cl_3^-}/(m_{Cl_2}\gamma_{Cl_2} m_{Cl^-} {}^{*}\gamma_{Cl^-})$

$E = E^{\circ}_G + (RT/2F)\ln p_{Cl_2} - (2RT/F)\ln(m\gamma_{\pm})_{HCl} + (RT/F)\ln(1 + K_1 p_{Cl_2})$

$(EF/RT) + 2\ln(m\gamma_{\pm})_{HCl} - \tfrac{1}{2}\ln p_{Cl_2} = (FE^{\circ}_G/RT) + K_1 p_{Cl_2} = \Psi$

$K_2 = (1 + K_1 p_{Cl_2})/\gamma_{Cl_2}(m_{Cl_2\,tot} + m_{Cl_2\,tot}/(K_1 p_{Cl_2}) - m_{HCl})$

Results are summarized in Table 3 and the standard potentials of the chlorine electrode shown in Fig. 8, with an indication of the data available in the literature.

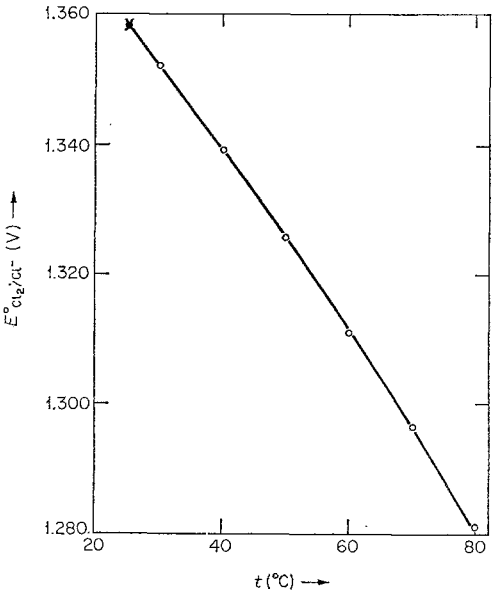

Fig. 8. Standard molar potentials of the Cl_2Cl^- electrode at various temperatures. Sources of data as indicated. ○ from [4, 6, 18]; × from [7, 22, 23, 24, 25, 26].

From the present determination of the equilibrium constants K_1 and K_2 it is verified that the formation of Cl_3^- ions has negligible effects when using reduced partial pressures of chlorine. Optimum conditions as far as the precision of the analysis of the chlorine–nitrogen mixture and the virtual absence of Cl_3^- ions in solution are concerned are obtained by working with 0·1 atm. of chlorine diluted with nitrogen. The specification of this optimum condition and the knowledge of the standard potentials of the chlorine electrode at various temperatures enabled us to use the hydrogen–chlorine cell for the emf-based determination of activity coefficients of hydrochloric acid at concentrations up to 11 molal and at temperatures up to 80°C (cf. Fig. 9).

All the required data being thus available, one can calculate the reversible potentials for the electrolysis of HCl solutions as functions of HCl concentration at various temperatures (Fig. 10).

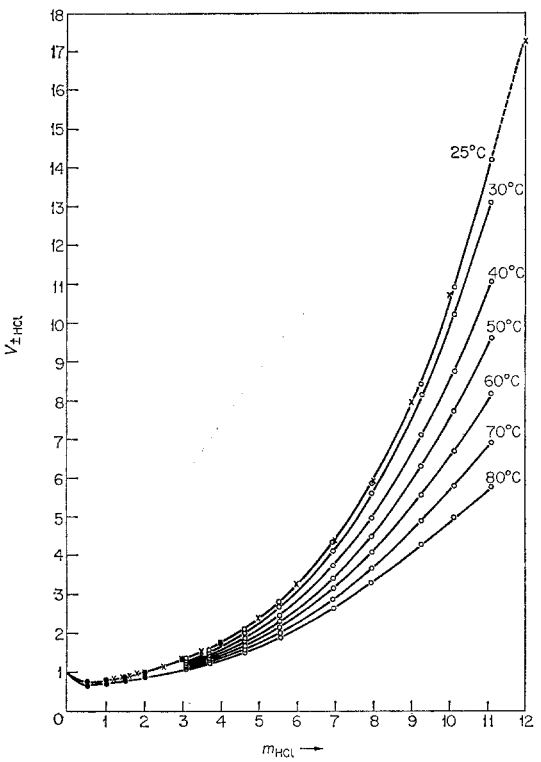

Fig. 9. Mean molal activity coefficients of aqueous HCl from various sources. ○ from [6]; × from [7]; ● from [5].

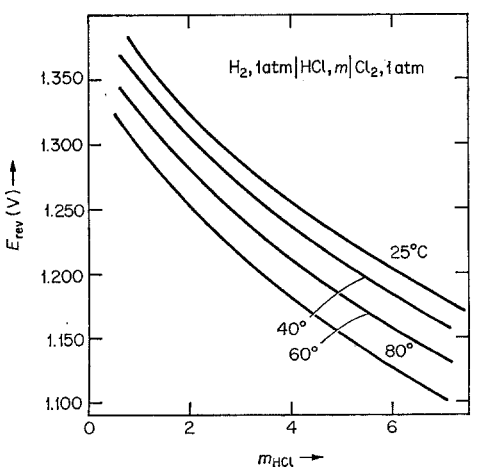

Fig. 10. Reversible voltages for the electrolysis of HCl at various concentrations and temperatures.

Thermodynamics of the processes of electrolysis in NaCl solutions

The basic experimental problem was mainly the setting up of a sodium amalgam electrode capable of working satisfactorily even at high

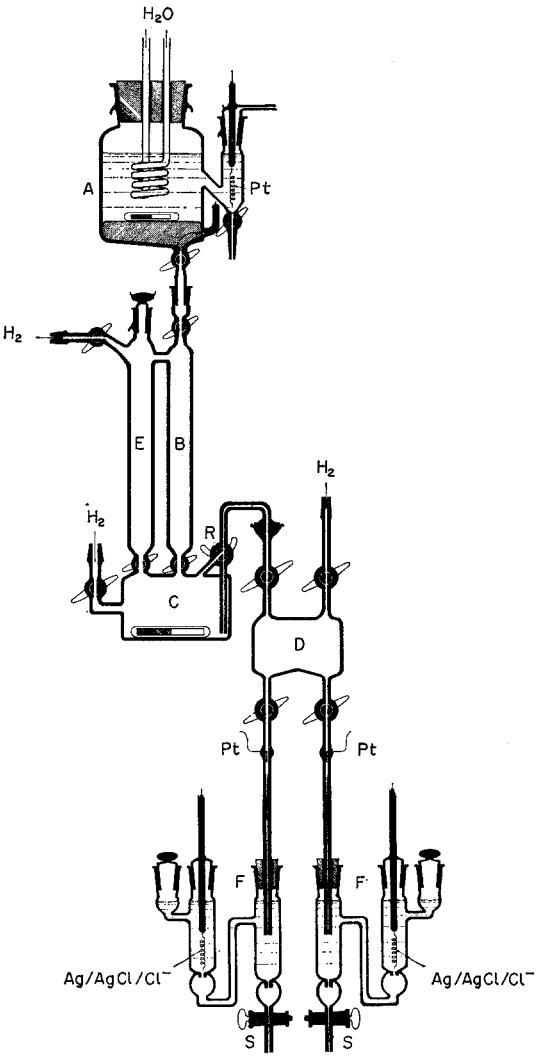

Fig. 11. Diagrammatic representation of the cell Me(Hg) MeCl/AgCl/Ag with details of the apparatus for preparation and storage of alkali metal Me amalgams. (From T. Mussini and A. Pagella, *J. Chem. Eng. Data*, **16** (1971) 49.)

temperatures. The electrode assembly adopted here has also served for studying thallium and calcium amalgams, and is of the flowing amalgam type [27], as shown in Fig. 11. The compartment for amalgam preparation and storage consists of a vessel A for the electrolytic production of the amalgam and of a vessel C for the dilution of the amalgam with pure mercury spilt from B and F, respectively. The amalgam, after mixing and storage in C, is transferred by hydrogen pressure into the vessel D which feeds the capillaries for the measurement cells F. Each of these cells

consists of the amalgam flowing from the capillary, of the NaCl solution and of the silver chloride electrode. The special shape of the bottom of each cell F permits us to avoid the decomposition of the amalgam dropped down to the bottom which could cause significant modifications of the NaCl solution composition.

From the emf of the above cell at various concentrations of NaCl in solutions and of sodium in the amalgams, it is possible to obtain the value of the standard potential $E^{\circ}_{Na(Hg)}$ of the sodium amalgam at each temperature of experiment, by a double extrapolation at $m_{NaCl} \rightarrow 0$ and at $x_{Na} \rightarrow 0$. Once $E^{\circ}_{Na(Hg)}$ is determined, the activity coefficients f_{Na} of sodium in the amalgam are readily obtained (see Fig. 12).

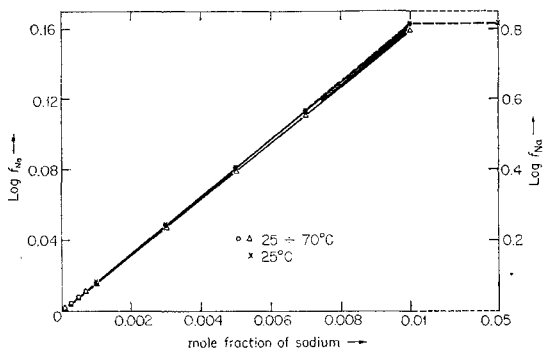

Fig. 12. Activity coefficients of sodium in amalgams. Sources of data as indicated: ○, △ from [14]; χ from [15].

On the basis of the combined knowledge of $E^{\circ}_{Na(Hg)}$ and f_{Na} it is then possible to obtain the activity coefficients of NaCl solutions shown in Fig. 13. Using the latter, it is possible to determine the transference numbers of NaCl (Fig. 14) from the emf's of a transference cell formed by two silver-chloride electrodes dipping into two NaCl solutions at different concentrations. Knowledge of all these data is necessary for the interpretation of the processes of electrical and mechanical transport through diaphragms in diaphragm cells and across the cathodic limiting layer in mercury cells.

The combined knowledge of the standard potentials of chlorine and sodium amalgam, and of the activity coefficients of sodium amalgams and NaCl solutions allow us to calculate the reversible potentials for a mercury cell corresponding to the conditions of cell inlet and cell outlet (Table 4).

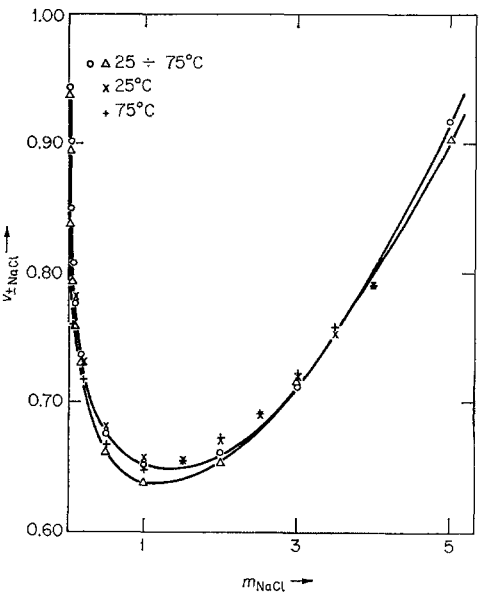

Fig. 13. Mean molal activity coefficients of NaCl. Sources of data as indicated: ○, △ from [10]; × from [11]; + from [9].

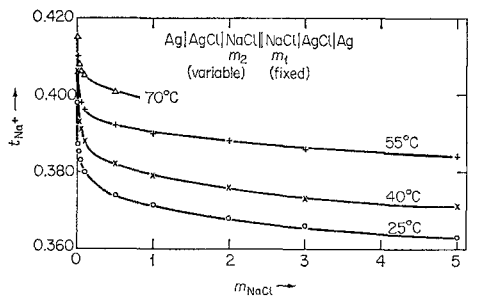

Fig. 14. Cation transference number of aqueous NaCl at various concentrations and temperatures. (From T. Mussini *et al.*, *Chemica e Industria* **52** (1970) 1187.)

With the same cell assembly as above, the activity coefficients of calcium amalgams [27] and of $CaCl_2$ solutions [10] have also been measured. Thus it is possible to calculate the potentials for the cathodic discharge of Ca^{++} ions from $CaCl_2$ (0·75 g/l) at 70°C; in the case of a calcium amalgam containing 2 ppm Ca, the Ca^{++} discharge potential is −1·919 V (NHE), only 45 mV more negative than the discharge potential of Na^+ corresponding to the conditions of the cell outlet (200 g/l NaCl). It is now evident that any factor leading to an excessive impoverishment of the brine may cause the simultaneous discharge of sodium and calcium.

Table 4. Reversible voltages for the electrolysis of NaCl solutions in mercury cells

	Concentration of NaCl in brine	*Concentration of Na in amalgam*	E_{rev} *at 70°C, V* *anode*	*cathode**	*whole cell*
Inlet	310 g/l (5·3M)	0·001% w/w ($X_{Na} = 8{\cdot}7\times10^{-5}$)	+1·241 NHE	−1·677 NHE	2·918
Outlet	200 g/l (3·4 M)	0·2% w/w ($X_{Na} = 1{\cdot}71\times10^{-2}$)	+1·263 NHE	−1·874 NHE	3·138
	240 g/l (3·65 M)	0·2% w/w ($X_{Na} = 1{\cdot}71\times10^{-2}$)	+1·256 NHE	−1·867 NHE	3·123

* These values can be compared with the reversible potentials for the cathodic discharge of calcium, to form a calcium amalgam from a calcium chloride solution at 70°C. see below

Concentration of $CaCl_2$ solution	*Concentration of Ca in calcium amalgam*	*Reversible potential for the discharge of Ca*
0·75 g/l	10 ppm	−1·942 V (NHE)
0·75 g/l	5 ppm	−1·932 V (NHE)
0·75 g/l	2 ppm	−1·919 V (NHE)

Anodic discharge of chlorine

Types of electrodes

During the last few years some important advances in caustic-soda technology have been made in connection with the introduction of new anode materials based on titanium supports. The advantages of the new (so-called 'permanent') anodes arise because they are non-consumable and, moreover, they do not need a continuous regulation of the inter-electrode distance. In addition titanium anodes can be obtained in peculiar geometrical forms (e.g. expanded metals) which are especially suitable for the chlorine evolution and rapid separation from the solution [28, 29, 30].

The new electrode materials for the brine electrolysis came from two research lines, one of which led to the titanium electrodes coated with noble metals of the platinum group (especially Pt, Pd, Ir, Rh), and the other led to the titanium electrodes coated with oxides of noble metals (particularly Ru and Ir). Literature on the kinetics of the anodic discharge of chlorine [31, 32, 33, 34] does not provide an exhaustive interpretation of the industrial chlorine processes because of the undervaluation of the slow phenomena of electrode passivation occurring at high current densities for very long times. One should indeed recall that the current densities for the chlorine discharge in some cases can now reach 1·5 A/cm^2 and thus produce tumultuous evolutions of gas, which lead to several difficult experimental problems. In the author's laboratory systematic researches were carried out on the anodic evolution of chlorine, using a rotating disc electrode which permitted a rapid removal of the gas bubbles and a control of the mass transfer processes. Under these conditions, it was possible to obtain stable and reproducible currents and potentials even when working at 0·3 A/cm^2 current densities. Measurements were freed from ohmic drop errors by using the usual oscillographic method based on current interruption.

Platinum and platinum-alloys electrodes

The first problem concerns the passivation phenomena accompanying the discharge of chlorine at pure platinum anodes, as shown in Fig. 15. It is seen that (i) the anodic potential for the chlorine evolution at platinum rapidly increases with increasing current density (curve A); (ii) the potential increase is irreversible; (iii) at high current densities the potential continues to increase slowly with time (curve C). The

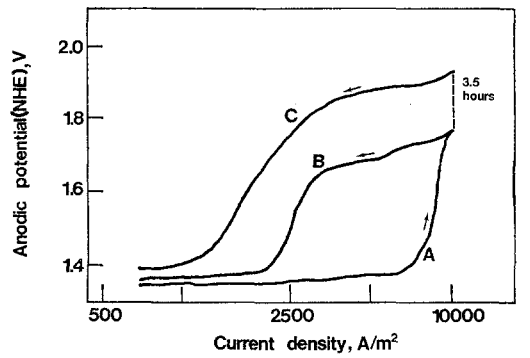

Fig. 15. Phenomena of platinum passivation during anodic discharge of chlorine from a saturated NaCl solution at 70°C. (From G, Bianchi, *Atti Giornate Chimica, Milano*, 1963). Curve A: obtained by increasing current densities. Curve B: obtained by decreasing current densities. Curve C: obtained by decreasing current densities, the electrode having however previously worked at 10,000 A/m² for 3·5 h.

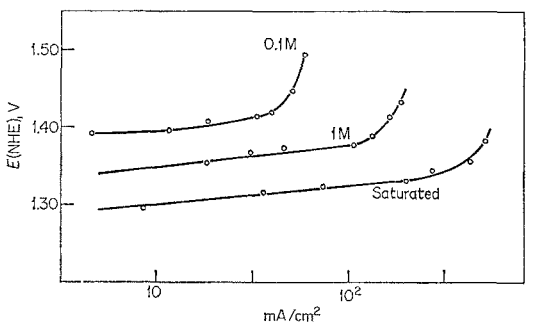

Fig. 16. Influence of NaCl concentration on the passivation of titanium–platinum electrodes. Solution pH = 3 (temperature 30°C) with a gaseous phase containing 1% Cl_2. Rotation speed of rotating-disc electrode (10 mm diameter) was 2,800 rpm.

platinum passivation is not favoured by low pH values [34] and high concentrations of chloride ions (Fig. 16). Fig. 17 further shows that the platinum passivation begins to arise even at 0·1 to 0·2 V overvoltages and becomes complete at 0·5 overvoltages. In the 0·2–0·5 V overvoltage range the platinum passivation establishes itself more rapidly, at a given overpotential, when the high rotation speed of the rotating electrode makes the mass transfer phenomena between solution and electrode surface faster. One explanation of these phenomena could well be that the platinum passivation is not caused by a direct discharge of OH^- ions, in which case it should be independent of mass transfer phenomena in solution, but by ClO^- ions getting on the platinum surface where they form oxychlor-

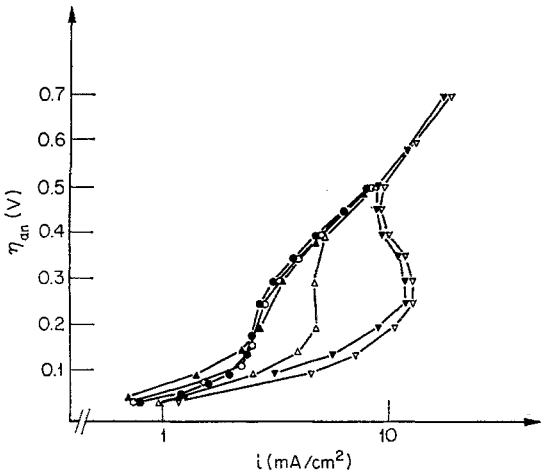

Fig. 17. Influence of diffusional phenomena on the passivity of Ti–Pt electrodes, depending on the NaCl concentration and the rotation speed of the rotating-disc electrode. Supporting electrolyte: 1 M $HClO_4$ at 30°C, in contact with a gaseous phase containing 1% Cl_2. (From G. Faita *et al*, *J. Electrochem. Soc.*, **116** (1969) 928.)

● 0·02 NaCl m = 850 rpm electrode: Ti/Pt
○ 0·02 NaCl m = 2,800 rpm electrode: Ti/Pt
△ 0·07M NaCl m = 850 rpm electrode: Ti/Pt
▲ 0·07M NaCl m = 2,800 rpm electrode: Ti/Pt
▽ 0·14M NaCl m = 850 rpm electrode: Ti/Pt
▼ 0·14M NaCl m = 2,800 rpm electrode: Ti/Pt

ides directly [37]. Another explanation relies upon a mechanism of electrochemical oxidation of ClO^- ions to ClO_3^- leading to evolution of oxygen which may remain partly chemisorbed on the platinum surface:

$$6ClO^- + 6OH^- \rightarrow 2ClO_3^- + 4Cl^- + \tfrac{3}{2}O_2 + 3H_2O + 6e$$

(E_{rev} = 0·7 V, NHE).

In any case the platinum passivation depends on the ClO^- ion concentration in the bulk solution ($Cl_2 + H_2O \rightarrow ClO^- + Cl^- + 2H^+$, pH dependent) as well as on ClO^- ion transport onto the electrode surface. In the case of pure iridium electrodes the passivity phenomena disappear; in the case of platinum–iridium alloys the passivity phenomena attenuate with increasing iridium percentage as shown by the results in Fig. 18. The different behaviours of platinum and iridium can be explained by considering the oxygen chemisorption at platinum to be characterized to some extent by irreversibility, which is not the case for iridium and platinum–iridium alloys [38].

The voltammetric sweeps in Fig. 19 clearly

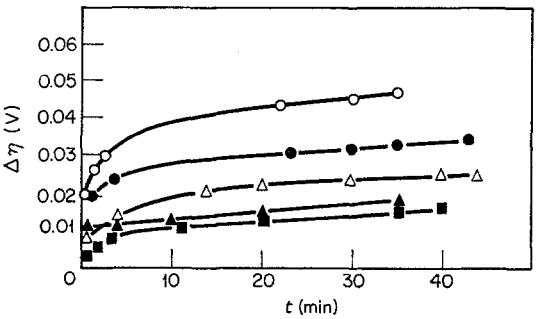

Fig. 18. Anodic overpotential as a function of time in a 0·1 M NaCl solution at pH = 3 and at 30°C, in contact with a gaseous phase containing 1% Cl_2. Rotation speed of the rotating-disc electrode was 2,800 rpm. Constant current density = 8 mA/cm²; ○ = Ti/Pt; ● = Ti/Pt-Ir (0·5%); △ = Ti/Pt–Ir (2%); ▲ = Ti/Pt–Ir (4%); ■ = Ti/Ir. (From G. Faita *et al.*, *J. Electrochem. Soc.*, **117** (1970) 1333.)

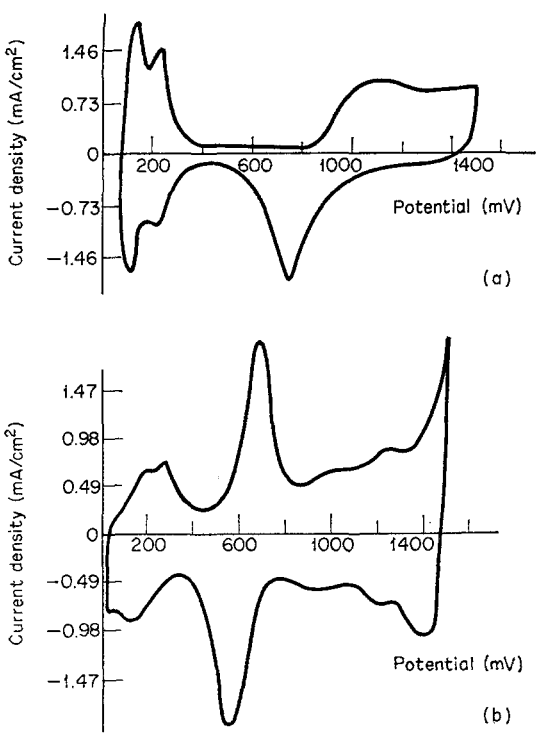

Fig. 19. Voltammetric sweeps (0·5 V/sec) in 2·3 M H_2SO_4 at 25°C. (a) platinum electrode; (b) iridium electrode. (From M. W. Breiter, *Electrochim. Acta*, **5** (1961) 145.)

show that at iridium electrodes the anodic formation and the subsequent cathodic reduction of chemisorbed oxygen occur at nearly equal potentials (correspondence of anodic and cathodic currents, at 0·8 to 1·4 V). In the case of platinum, however, the anodic currents are zero until the potential falls to 0·9 V. In other words, within the 0·9–1·4 V range, chemisorbed oxygen gradually accumulates on platinum since in that potential range a chemisorbed oxygen formation, but no reduction, can take place.

It was shown [39] that the anodic evolution of chlorine at either non-passive platinum or platinum–iridium alloys occurs following the scheme:

(a) $Cl^- \rightarrow Cl_{ads} + e$

(b) $2Cl_{ads} \rightarrow Cl_2$,

the step (b) being rate-determining, with a Tafel slope of 0·030 V/decade. The irreversible oxygen chemisorption takes up sites on the electrode surface making them unavailable for the (b) chlorine evolution reaction, a 2nd order process with respect to Cl_{ads} (i.e. to the sites) which is thus necessarily markedly slowed down. In the case of the anodic chlorine discharge from acid solutions, the surface coverage by chemisorbed oxygen is quite small even for platinum electrodes, thus step (b) is fast and step (a) becomes rate-determining [40]. Although a small amount of iridium suffices to prevent the platinum passivation, in practice higher iridium amounts (20–30%) are used to obtain electrodes of high chemical resistance. Fig. 20 confirms that only

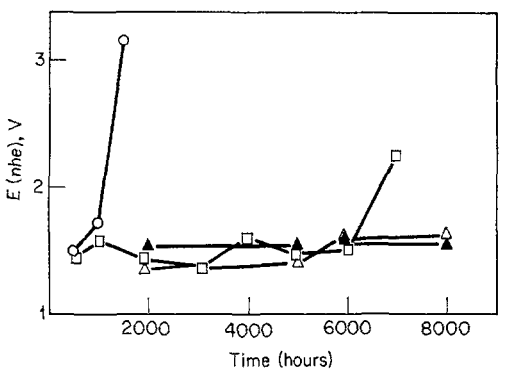

Fig. 20. Time dependence of the anode potential for the evolution of chlorine. Constant current density = 1 A/cm²; NaCl = 310 g/l; pH = 3; T = 70°C; ○ = Ti/Pt–Ir (5%); □ = Ti/Pt–Ir (10%); △ = Ti/Pt–Ir (20%); ▲ = Ti/Pt–Ir (30%). (From G. Faita *et al.*, *J. Electrochem. Soc.*, 117 (1970) 1333.)

with iridium amounts greater than 20% is it possible to obtain electrodes whose potentials remain constant even over electrolysis times of thousands of hours.

When electrolysing HCl solutions [41] cor-

rosion phenomena at anodes are more severe and the maximum chemical resistance is obtained with 45% iridium–platinum electrodes [4].

Titanium-based oxide electrodes

The second research line concerned titanium electrodes with oxide coatings (particularly ruthenium oxide) showing metallic-type conductivity. The titanium support apart, this idea is not completely new, as cast magnetite electrodes were already largely in use in caustic-soda plants before graphite electrodes gained ground. Fig. 21 illustrates the electrical conductivities of

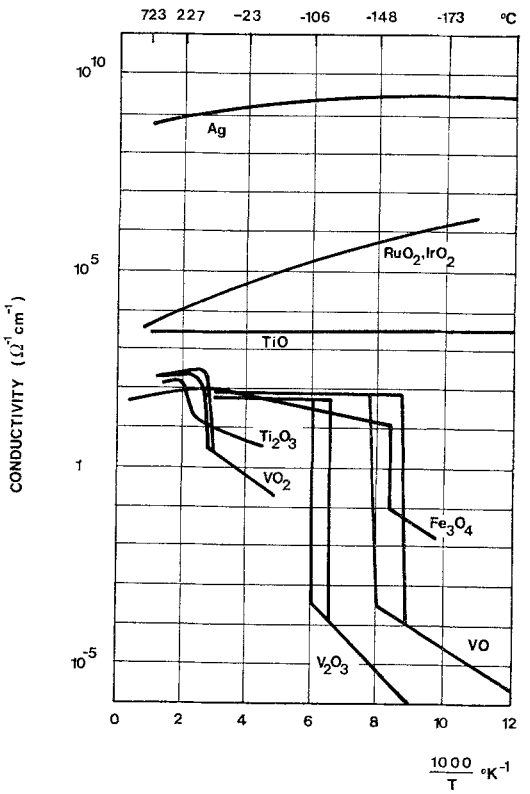

Fig. 21. Transition metal oxides with metallic conductivity. Data from [42] for Fe_3O_4; from [43] for IrO_2 and RuO_2; all other data from [44]. Electrical conductivity of silver is reported for comparison purposes.

some metal oxides, as contrasted with the conductivity curve for a typical metal, silver. It is seen that ruthenium, iridium and titanium oxides have negative temperature coefficients for the electric conductivity (this is typical of a metal-type conductance) within the whole temperature range. For other oxides such as magnetite and Ti_2O_3 the metal-type conductance only occurs at temperatures much higher than room temperature. At lower temperatures there is a transition, and these oxides behave as semiconductors with positive temperature coefficients of the conductance (activated conduction). Other oxides having a metallic behaviour and showing a transition with decreasing temperature are the vanadium oxides (VO, V_2O_3 and VO_2).

From this survey, the striking attractiveness of the ruthenium, iridium and titanium oxides for the realization of electrodes for the anodic discharge of chlorine is obvious. Indeed, their electronic conductance is accompanied by a strong chemical inertia which is related to the absence of an electric field penetrating inside the oxide influencing lattice bonds. The chemical adsorption of anion, i.e. the first step for the subsequent chemical attack, may take place preferentially on the cationic positions of the oxide. In the case of an oxide with no electronic conduction, the anion adsorption leads to a surface with a localized electric charge which can weaken the neighbouring lattice bonds, whereas in an electronic-conduction oxide the electric charge of the adsorbed species is uniformly distributed and shared in the bulk oxide. The electronic conduction also removes electric gradients in the bulk oxide and hinders any anionic migration which could, in the long term, lead to a breakdown of the oxide lattice structure. From the electrodic standpoint, it was shown that the anodic discharge of chlorine at RuO_2 electrodes proceeds along an electrochemical–chemical mechanism quite analogous to that observed at non-passive platinum or iridium which implies the intervention of the Cl_{ads} species. The RuO_2 electrode properties and performances depend on the preparation methods (materials, i.e. $RuCl_3$; temperatures; oxygen partial pressures) as shown by studying the behaviour of appropriate redox systems [45, 46, 47, 48]. This fact leads us to believe that the RuO_2 electrode behaviour might be significantly affected by both some stoichiometric imbalance and the transition between the metallic behaviour (orbitals overlapping) to the semiconductor behaviour. It was shown that the behaviour of bulk RuO_2 is different from that of RuO_2 in the form of a film ob-

tained by thermal decomposition [49], see Fig. 22. An interesting feature is that the temperature coefficient of the electric conductivity of RuO_2 deposited as a thin film on silica corresponds to a semiconductor's behaviour (activated conductivity) in the very range of temperature where RuO_2 electrodes find industrial applications.

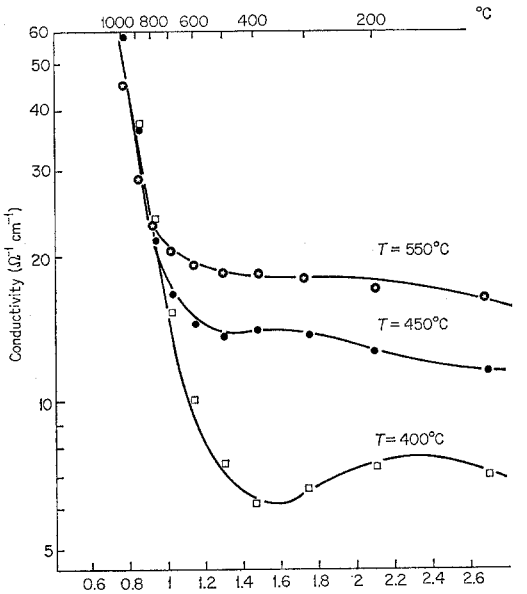

Fig. 22. Electrical conductivity of RuO_2 film on silica for different temperatures of decomposition (From S. Pizzini, Paper No. 32 presented at the Fall Meeting of the Electrochemical Soc., Atlantic City, N.Y., October 1970).

Even the morphology of the RuO_2 film surface is markedly affected by both the preparation temperature and the substrate nature [50]. For deposits obtained by thermal decomposition of $RuCl_3$ on silica at 450°C, it is seen that the film has a honeycomb structure, where the single cells are separated by narrow and deep channels (Fig. 23; ESM × 3000). The interior of any single cell is empty (or partially filled with amorphous material) as one can observe in the same figure, where the inside of a cell is also shown. The porosity of the walls of the cells increases (Fig. 24: ESM × 3000) as the temperature of preparation (or of annealing) increases and large cracks appear, mainly on the upper walls of the cells. At this temperature (~850°C) small single crystals begin to grow in the channels between cells, up to a size of tens of μm, provided that enough time elapses. X-ray diffraction patterns confirm that the RuO_2 deposits obtained by thermal decomposition at lower temperatures (≃500°C) are amorphous, the crystalline habit appearing only after long annealing at ~800°C.

Many problems concerning properties of oxide-based electrodes (including the so-called 'bronzes') are still open to speculation. However it already seems clear that these new electrodes did introduce an innovation even into the most classical electrochemical technologies, such as that of caustic-soda.

References

[1] R. G. Milner and T. C. Jeffery, *J. Electrochem. Soc.*, **117** (1970) 353 C.
[2] Chimica E Industria, *Chimica e Industria* **52** (1970) 999.
[3] Noyes, *Chlorine and Caustic Soda Manufacture*, Noyes Development Corp. London (1969).
[4] G. Faita, P. Longhi and T. Mussini, *J. Electrochem. Soc.*, **114** (1967) 340.
[5] H. S. Harned and R. W. Ehlers, *J. Am. Chem. Soc.*, **55** (1933) 2179.
[6] A. Cerquetti, P. Longhi and T. Mussini, *J. Chem. Eng. Data*, **13** (1968) 458.
[7] M. Randall and L. E. Young, *J. Am. Chem. Soc.*, **50** (1928) 989.
[8] G. J. Janz and A. R. Gordon, *J. Am. Chem. Soc.*, **65** (1943) 218.
[9] R. P. Smith and D. S. Hirtle, *J. Am. Chem. Soc.*, **61** (1939) 1123.
[10] T. Mussini and A. Pagella, *Chimica e Industria*, **52** (1970) 1187.
[11] H. S. Harned and L. F. Nims, *J. Am. Chem. Soc.*, **54** (1932) 423.
[12] G. Scatchard and S. S. Prentiss, *J. Am. Chem. Soc.*, **55** (1933) 4855.
[13] R. W. Algood and A. R. Gordon, *J. Chem. Phys.*, **10** (1942) 124.
[14] T. Mussini, A. Maina and A. Pagella, *J. Chem. Thermodynamics*, **3** (1971) 281.
[15] H. Dietrick, E. Yeager and F. Hovorka, Techn. Report No. 3 ONR Contract 581 (00), Western Reserve University (1953).
[16] G. Bianchi, A. Barosi, G. Faita and T. Mussini, *J. Electrochem. Soc.*, **112** (1965) 921.
[17] G. Bianchi, *J. Electrochem. Soc.*, **112** (1965) 233.
[18] A. Cerquetti, P. Longhi, T. Mussini and G. Natta, *J. Electroanal. Chem.*, **20** (1969) 411.
[19] G. Charlot, 'Oxidation–Reduction Potentials', Pergamon, London (1958) p. 9.
[20] M. S. Sherrill and E. F. Izard, *J. Am. Chem. Soc.*, **53** (1931) 1667.
[21] G. Zimmermann and F. C. Strong, *J. Am. Chem. Soc.*, **79** (1957) 2063.

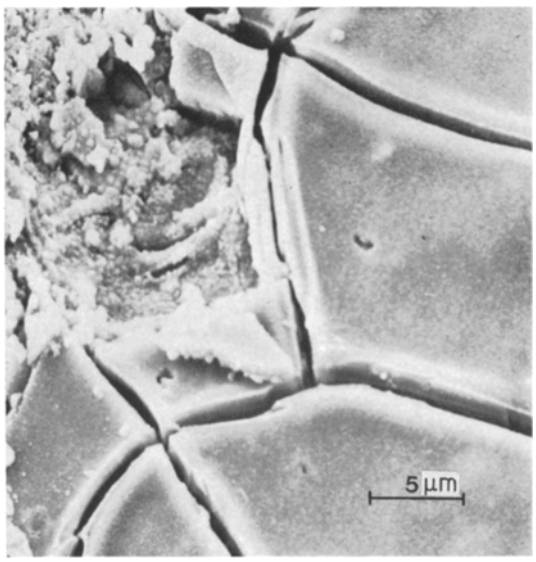

Fig. 23. Microphotography taken by ESM on the surface of a RuO_2 film prepared at 500°C. (From G. Bianchi and S. Pizzini, *Proc. 2nd Int. Conf. on Materials Science*, Tremezzo, Como, September 1970, in press.)

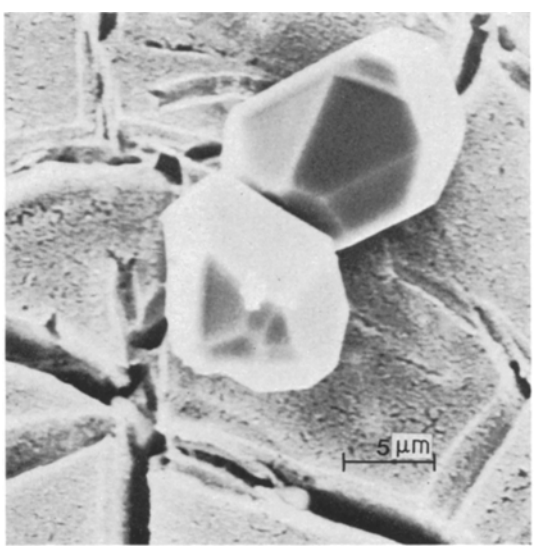

Fig. 24. Microphotography taken by ESM of RuO_2 film annealed at 850°C for 2h. (From G. Bianchi and S. Pizzini, *Proc. 2nd Int. Conf. on Materials Science*, Tremezzo, Como, September 1970, in press.)

[22] E. Müller, *Z. Physik. Chem.*, **40** (1902) 158.
[23] A. Schmid, *Helv. Chim. Acta*, **7** (1924) 370.
[24] J. Forbes, S. W. Glass and R. M. Fuoss, *J. Am. Chem. Soc.*, **47** (1925) 2892.
[25] M. Kameyama, H. Yamamoto and S. Oka, *J. Soc. Chem. Ind.* (Japan) **29** (1926) 679.
[26] E. Wilke and O. Kieninger, *Z. Physik. Chem.*, **116** (1925) 215.
[27] T. Mussini and A. Pagella, *J. Chem. Eng. Data*, **16** (1971) 49.
[28] V. de Nora and A. Nidola, Paper No. 270 presented at the Spring Meeting of the Electrochemical Society, Los Angeles (15 May 1970).
[29] O. de Nora, *Chem. Eng. Tech.*, **42** (1970) 222.
[30] C & EN, Nov. 9, 1970, p. 32.
[31] F. T. Chang and H. Wick, *Z. Phys. Chem.*, **172** (1935) 448.
[32] G. Teodorase, *Z. Phys. Chem.*, **33** (1959) 129.
[33] S. Toshima and H. Okaniwa, *Denki Kagaku*, **34** (1966) 641.
[34] E. L. Littauer and L. L. Shreir, *Electrochim. Acta*, **11** (1966) 527.
[35] G. Bianchi, *Atti Giornate Chimica*, Milano (1963).
[36] G. Faita, G. Fiori and J. W. Augustynski, *J. Electrochem. Soc.*, **116** (1969) 928.
[37] D. G. Peters and J. J. Lingane, *J. Electroanal. Chem.*, **4** (1962) 193.
[38] M. W. Breiter, *Electrochim. Acta*, **5** (1961) 145, 169.
[39] G. Faita, G. Fiori and A. Nidola, *J. Electrochem. Soc.*, **117** (1970) 1333.
[40] T. Yokoyama and M. Enyo, *Electrochim. Acta*, **15** (1970) 1921.
[41] G. Bianchi and T. Mussini, *Ricerca Scientifica*, **34** (IIA) (1964) 37.
[42] D. S. Tannhauser, *J. Phys. Chem. Solids*, **23** (1962) 25.
[43] W. F. Ryden, A. W. Lawson and C. C. Sartain, *Physics Lett.*, **26A** (1968) 209.
[44] J. B. Goodenough, *Proc. Int. Conference on Materials*, Schatz (Ed.) New York (1968).
[45] G. Tantardini, Thesis, University of Milan (1968).
[46] D. Galizzioli, Thesis, University of Milan (1969).
[47] G. Buzzanca, Thesis, University of Milan (1970).
[48] S. Trasatti and G. Buzzanca, *J. Electroanal. Chem.*, **29** (1971) App. 1–5.
[49] S. Pizzini, Paper No. 32 presented at the Fall Meeting of the Electrochemical Society, Atlantic City, N.Y. (October 4–9, 1970).
[50] G. Bianchi and S. Pizzini, *Proc. 2nd Int. Conference on Materials Science*, Tremezzo, Como (13–25 September 1970) in press.